EAI Endorsed Transactions
on Ai and Robotics
Research Article EAI.EU

Prediction of short circuit current of wind turbines based on artificial neural network model

Ali AbdulKarim AbdulRahim[1], Ebrahim Aghajari[2,*]

[1]Department of Electrical Engineering, Ahvaz Branch, Islamic Azad University, Ahvaz, Iran
[2]Department of Electrical Engineering, Ahvaz Branch, Islamic Azad University, Ahvaz, Iran

Abstract

The growth of renewable energy on a global scale is making significant strides in power plants. This is due to the increasing concern about climate change, the rising demand for electricity, and the necessity to reduce reliance on fossil fuels. Ensuring the successful integration of new energy resources into the existing network is just as crucial as it requires the system to be reliable and adaptable. For instance, wind energy, which is one of the renewable sources, has an intermittent nature that necessitates the ability to synchronize its actions to achieve the desired system performance. The objective of this study is to utilize a new neural network system to calculate the short circuit current of power plants. Specifically, the focus is on identifying and categorizing the short circuit faults that occur between the stator coils of the squirrel cage induction generator used in wind power generation. To achieve this, a system was developed to simulate turbine data. Subsequently, four feature extraction techniques and machine learning algorithms were employed to enable early detection of short circuit faults. The numerical results obtained from the simulation demonstrated the high efficiency and accuracy of the proposed model. This research is based on a valid approach for early detection of short circuit in the stator winding in induction generators used in wind turbines. Using a wind turbine test location, we introduced different types of short circuit in the generator. We proposed to use four feature extraction technical along with three categories.

Keywords: Power Plant, Short Circuit Current, Neural Network.

Received on 20 03 2024, accepted on 20 06 2024, published on 17 07 2024

doi: 10.4108/airo.5955

1. Introduction

Advances in technology for the optimal extraction of energy from renewable sources, along with cost reductions and government policies with financial incentives that support the growth of renewable energy, have led to a significant integration of renewable energy sources. For example, a new energy agreement was reached in Denmark in March 2012 which includes initiatives to bring Denmark closer to the goal of 100% renewable energy in the energy and transport sectors by 2050. Ontario's Green Energy and Green Economy Act of 2009 created a feed-in program that provides payment for renewable energy production above the market price. As the installed capacity of wind generation continues to grow, it is necessary for facility engineers to be aware of the behavioural characteristics of wind farms and the effects they have on the power grid, and this growth presents unique challenges for the proper integration of wind energy into the power grid [1].

A unique aspect of wind generation that separates it from conventional generation is its short circuit behaviour. Wind turbines typically use an induction generator that is either directly connected to the grid or decoupled from the grid via power electronics. These topologies have different short-circuit characteristics compared to concurrently connected machines. Appropriate short-circuit studies are necessary to determine that the maximum short-circuit contribution of a given machine is within the range of the

*Corresponding author. Email: eaghajari88@iau.ac.ir

circuit breakers and that the protective devices are properly matched. It is very important to study the impact of systems before integrating any new generation into the existing power grid, and studies of short-circuit participation are a critical task. Short-circuit levels must be evaluated for accurate design of protective relay settings, equipment ratings, and protection coordination. Since the accuracy of relay settings is very important to prevent relays from malfunctioning, accuracy in short-circuit levels and thus short-circuit models is very important [2].

In order to evaluate the behaviour of wind generators and their response to system faults, appropriate wind generator models must be created. Short circuit faults can occur in the power system for various reasons, of which line-to-ground fault is the most common. The short-circuit characteristics of synchronous machines are well defined because the technology has existed for several years and accurate models are available to predict their short-circuit contribution. However, this is not the case with wind turbine technology, which is relatively new and constantly evolving. [3].

Several techniques have been proposed in the literature to model the short circuit behaviour of wind turbine generators. The first generation of utility-sized wind turbine generators were Type I wind generators based on a squirrel cage induction generator with blade pitch angle control as the only wind power control mechanism [4]. This design has the advantages of mechanical simplicity, high efficiency and low maintenance requirements [5]. Jiménez-Buendía, Francisco et al. [6] further show that Type 4 wind generators can be represented by a current source with upper and lower limits based on the power converter rating for short-circuit analysis.

VDNE, a nonwrite equivalent, augments the classical voltage source with an additional flow component to the voltage. To address the nonlinear relationship between the VDNE's output and the terminal voltage, repeated recalculations of the short-circuit connection within the network are necessary.

The results of entire network's EMT analysis, after reaching a steady state, are used as a reference solution. These results are compared with the approximations used by VDNE in the frequency domain. Preliminary findings indicate that the combined VDNE and network solutions align well with the actual network behavior.

In this study, the external network is modeled using a Thévenin equivalent. While a detailed model could be created, it is important to identify the nonlinear current source component of the VDNE, considering the wide range of impedance characteristics observed in the Point of Entry (POE) [7].

The method involves an initial step where an EMT model is validated using a zero percent three-phase voltage gradient field experiment. The EMT model then represents the worst-case scenario for short-circuit current. The resulting time series fits an equation representing the short-circuit current contribution as AC and DC decay components. This confirms the primary symmetrical short-circuit current. However, it was found that both the peak short-circuit current and the thermal equivalent are not accurately calculated. To address this, F. Jimenez-Buendía et al. [8] proposed an alternative calculation method, yielding relatively accurate results.

Kumar et al. [9] reviewed various analytical methods designed to solve the problem of locating and sizing distributed generation sources to avoid voltage deviations. Niaki et al. [10] emphasized that studying AC load distribution is essential for solving the placement problem. They noted that the optimal load distribution method makes the problem nonlinear, complicating the determination of the unit's output power and leading to multiple local optimal solutions. Consequently, finding the most optimal solution with this method presents challenges, suggesting that random exploratory methods could be beneficial for future research. Shuaibu et al. [11]

Methods such as the Particle Swarm Optimization (PSO) algorithm, bee colony optimization, neural network algorithms, and genetic algorithms have been applied to solve the problem of determining the optimal location and size of distributed generation sources. These methods focus on the dual objectives of minimizing losses and production costs for two types of distributed production. Dehghani et al. [12] presented a hybrid method combining the colonial competition algorithm with a genetic algorithm to address the optimal placement and sizing of both parallel capacitor banks and distributed generation sources simultaneously.

Karunarathne et al. [13] discussed the optimization and related issues of having multiple distributed production sources operating in various modes [14,15]. They concluded that the availability and connection point of a distributed generation source could significantly impact the output of other resources in the network. The proposed method aims to maximize the output capacity of scattered production resources under these conditions.

Ghotbi et al. [16] highlighted that the ideal tripping characteristic of distance relays is influenced by the mutual effect of parallel transmission lines. They considered the relay performance threshold settings for lines connected to wind farms to be affected by continuous voltage fluctuations in parallel transmission lines. They proposed a solution for setting the distance relay in parallel lines within a network connected to a wind farm.

Therefore, in accordance with the common issues discussed in recent research, it can be seen that when the distributed generation is connected, the short circuit level of the network changes and the settings of the protection system equipment must be altered; if the distributed generation is disconnected from the network, the settings must return to the initial state. To achieve this goal, many connections are needed, which are usually not available in distribution networks. To solve this problem, a coherent plan is required to protect distribution networks via scattered generation sources. The lack of proper placement of scattered generation power plants in such a network causes an increase in power loss and increases the costs of energy production and transmission whilst disrupting protection systems, so it is necessary to use optimization methods to determine the optimal placement of these

power plants within the network. This approach will determine the number, installation locations, and capacities of distributed generation power plants to achieve the maximum reduction of disturbances in the existing grid protection systems, while considering the problem's constraints.

The purpose of this research is to calculate short circuit current in wind turbines using an artificial intelligence method. The structure and performance of the artificial intelligence network will be explored in its solving of non-linear mathematical problems. The problem will be coded using an artificial neural network during the training and testing phases, employing four different distribution networks with varying connection flows as input. During the test phase, the trained artificial neural network correctly determines the minimum short-circuit current error through multiple iterations for the test network. It then determines the value of the short-circuit current using an optimally weighted neural network. The numerical results obtained from the simulation will demonstrate the efficiency and accuracy of the proposed model.

2. Materials and Methods

2.1. Equations governing the circuit of wind power plant

A detailed description of the equalization method of a wind power plant for load flow studies is provided in the WECC wind power flow modeling guide reference [3]. Figure 1 shows a sample design of 18 wind turbine power plants. Determining the error contribution of a wind power plant in the transmission network can be done by reducing the power plant to the following circuit:

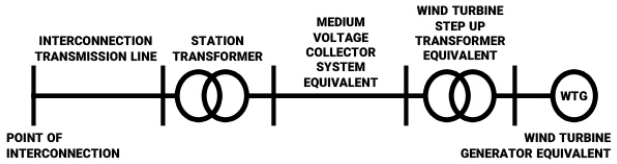

Figure 1. Wind power plant equivalent to a machine

The challenge is in calculating the equivalent impedance based on the components of the wind farm. Before calculating the equivalent impedance, a preliminary conversion of all impedances to a volt-ampere base (SBASE) must be done. The equation for converting impedance in units (pu) to a new base power (SBASE) is provided by the following equation:

$$Z_{pu\_new} = Z_{pu\_old} * (\frac{S_{BASE\_new}}{S_{BASE\_old}}) \quad (1)$$

One of the most challenging aspects of extracting the impedance of a wind power plant is reducing the collector system to an equivalent impedance. The method of equating the collector system of a wind power plant is documented in [4] and is calculated with the following equations:

$$Z_{eq} = \frac{\sum_{i=1}^{I} Z_i n_i^2}{N^2} \quad and \quad B_{eq} = \sum_{i=1}^{I} B_i \quad (2)$$

Where I is the number of branches in the collector system, Z_i and n_i are the impedance of the i-th branch, and N is the total number of wind turbines in the power plant.

Once the equivalent impedances of the components of a wind power plant are extracted, we can reduce the diagram of Figure 1 to an equivalent impedance value. For the entire wind power plant, the equivalent values of R and X can be found by summing the impedances of the individual components. Below is the equivalent impedance calculation for our example:

$$R_{eq} = R_{line} + R_{SUB\_XFMR} + R_{COLLECT} + R_{SU\_XFMR} \quad (3)$$

$$X_{eq} = X_{line} + X_{SUB\_XFMR} + X_{COLLECT} + X_{SU_{XFMR}} + X_{WTG} \quad (4)$$

Obtaining the equivalent short circuit diagram for the entire wind farm involves aggregating the current contributions of each wind turbine generator (WTG) and adjusting for the change in base. The equivalent short circuit conditions of a wind farm equipped with current limiting power converters along with corresponding current contribution from 18 type IV WTGs are obtained using the following relationships.

$$I_{SC\_plant} = \left(I_{SC_{plant}}.N\right).(\frac{S_{BASE\_new}}{S_{BASE\_old}}) \quad (5)$$

$$I_{SC\_plant} = (.1 * 18) * (\frac{2MVA}{100MVA}) = 0.39pu \quad (6)$$

Positive sequence impedances provide the worst case fault current for a balanced three-phase fault. Wind turbine generators are typically ungrounded, rendering them open circuits for zero-sequence current. In this research, the focus is on transmission-level errors within wind power plants. For this purpose, the zero-sequence equivalent at the connection point can be simplified to an open circuit, modeled as an infinite impedance. As a result, the WTGs do not introduce any zero-sequence fault current into the network.

The development of the equivalent machine for the entire wind power plant is done using ASPEN One-Liner short circuit software. ASPEN One-Liner is capable of demonstrating power electronics effects in Type III (w/chopper), and Type IV WTGs with a current-limiting generator model. Once the flow limits are defined for each

wind turbine and the appropriate adjustments are made on site, simulating a fault in the POI will produce the required values for an equivalent device. Table 1 shows the comparison of results in ASPEN with relations (5), (6).

Table 1. Comparison of methods for single machine equivalents (current limiting WTG)

	Section 4.7 Method	ASPEN One-Liner
3-Phase Fault Current	0.396pu	0.397pu

A single machine equivalent can now be modeled by limiting the power plant to an output current of 0.397 pu. It is equivalent to A166 at 100 KV - 138 MVA base.

2.2. Experiments and data collection

The wind turbine simulated in this work is based on the configuration described by Catalán et al. [17], which consists of a squirrel cage induction generator (SCIG), full-speed and full-variable-speed, i.e. electric. Figure 2 shows the facility where the experiments were conducted. National Instruments NI-USB-6009 data acquisition modules and a microcomputer are also on-site, where the LabVIEW interface runs for data acquisition.

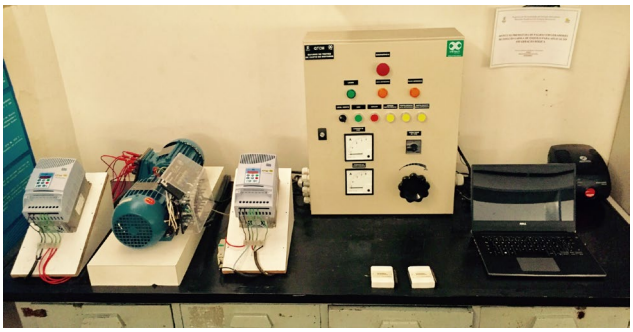

Figure 2. Installing the wind turbine system simulation bench: QTCM device and wind turbine simulation setup

The data collected with the proposed system contains information from the SCIG operating in different production regimes, subject to failure or non-operation. This enables the creation of a database where machine learning techniques are later applied for early detection of failures. The steps of conducting experiments in the simulation wind turbine system are shown in Figure 3. It should be remembered that fb is the frequency value commanded by MP converter and FG by SCIG.

2.3. Description of simulation process for wind turbine/induction generator

In this section, the steps of conducting tests in the simulated wind turbine system are described. It is necessary to remember that fb is the frequency value commanded by the MP and FG converter by the SCIG [18].

1. The acceleration and deceleration ramps of both drives are set to the same value. This prevents excess current in some electric machines during start-up.

2. Fb = FG is set to ensure that both cars are at the same speed after the start of the ramp.

3. Simultaneously, the start command is given to both frequency converters.

4. When the system is in constant operation, FG is gradually reduced to reach the first generation point.

5. Power supply to the SCIG converter is turned off.

6. Following the power cutout, the DC bus voltage of the generator frequency converter should be reduced, adjusting FG to reach 210V.

7. Data collection is done through the LabVIEW interface.

8. FG is incrementally reduced to fmax, until one of the following occurs:

   - ✓ The generator reaches the rated current.
   - ✓ The DC bus voltage of the converter, Vcc, reaches the maximum value allowed by the equipment, 380 volts.
   - ✓ The primary machine Imp reaches its rated current.

9. Step 7 is repeated as necessary.

10. Simultaneously, shutdown commands are issued to both frequency converters and operations are halted until the mechanical assembly comes to a stop.

11. New values are defined for fb and FG.

12. Repeat step 1 as part of the Materials and Methods.

2.4. Prototype Generator

The preparation of the machine was done in such a way that the development of the short circuit could be simulated, from the initial occurrence, almost imperceptible, to the extreme situations before the destruction of the stator winding.

Table 2. Summary of machine states considering high impedance (AI), low impedance (BI), with intensity levels equivalent to the percentage of short circuit cycles of 1.41%, 4.81% and 9.26%, for a total of 6 failure levels

Types of short circuit	Rounds %	Degrees of force
AI	1.41	1
	4.81	2
	9.26	3
BI	1.41	4
	4.81	5
	9.26	6

For data collection, a graphical interface was used in LabVIEW software from National Instruments, which was developed specifically for this program. The two data acquisition modules used were NI-USB-6009, of the same brand. This module has 14-bit resolution, 8 analog inputs, 4 of which are differential. For monitoring, 3 electric current sensors (current transformer (CT) type), a vibration sensor and an axial magnetic flux sensor were installed in the induction generator.

2.5. Experimental description of the generator

In order to determine to what degree the generator preparation process has changed the characteristics of the device, tests were performed on this generator and the data were compared with the samples obtained from the standard generator. Figure 4 shows the behaviour of the electric current, the voltage in the DC Bus of the converter and the power with the change in the frequency of the main device and the generator. The blue curves are the measurements taken on the standard generator, while the green curves are the modified generator curves. The frequency difference between GP and GM with the same output point is 0.5 Hz.

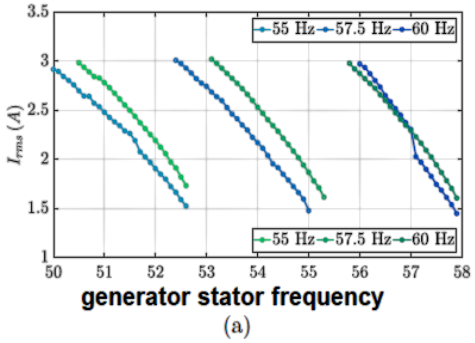

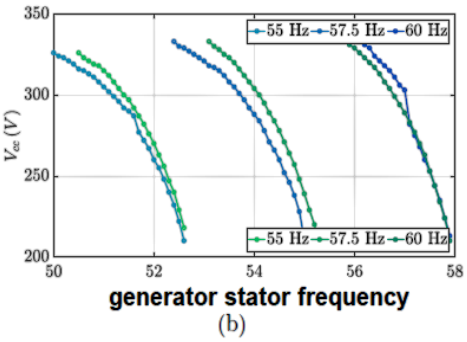

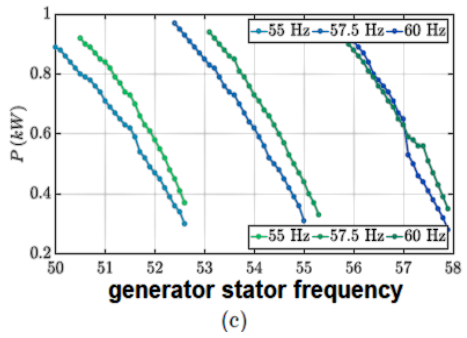

Figure 3. The behaviour of GP in blue and GM in green. In (a, electric current behaviour; b, DC Bus voltage and c, three-phase power is produced

This evidence has helped guide experiments to collect generator data. For fb between 45 and 60 Hz, the interval is 2.5 Hz and for FG steps it is defined as 0.02 Hz. The experiments were divided into 7 groups. A total of 1356 data acquisitions have been made, of which 248 are normal generator conditions and 1108 are failure conditions. Table 3 summarizes the experiments.

Table 3. The steps of conducting experiments in the induction generator

Step	fb	fg
Normal	45 to 60Hz Steps of 2.5Hz	f_1 = (V_{cc} = 210V) until f_{max} = (V_{cc} = 380V or I_g = 3A or I_{mp}=3A), with steps 0.02Hz
Failure AI-1		
Failure AI-2		
Failure AI-3		
Failure BI-1		
Failure BI-2		
Failure BI-3		

3. Evaluation and validation of results

According to the scientific literature search, the MCSA technique was used to use generator electric current signals to form a database to detect short circuit faults between induction machines. Figure 5 shows a comparison between the SCIG signal collection operating near the nominal current also under normal and Bi-3 conditions. The base frequency is 60 Hz, the generator frequency is 58.87 Hz with respect to no failure and 58.84 Hz for the generator with failure. After placing the short circuit between the R and T phases, we found that there is an imbalance between the electric currents of the three phases of the generator, as seen in Figures 5a and 5b. In Table 4, this comparison between the measured electric current values in the converter line generator is shown, and it is found that the occurrence of short impedance, both high and low, unbalances the system, and this in the sub-regulator and current overflow in other phases are inevitable. Also, both the DC Bus power and voltage have decreased in their nominal values, also indicating the occurrence of abnormality.

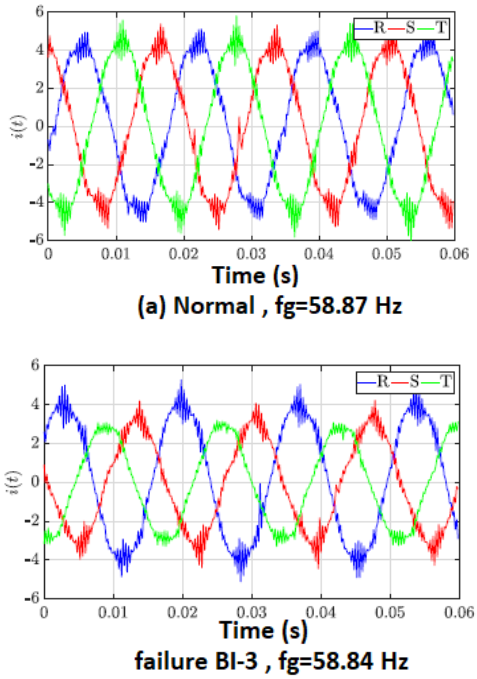

Figure 4. Natural generator with failure BI-3, with Hz = 60 fb

Table 4. Numerical comparison between electric line current values, DC Bus voltage and power for normal condition

Measured values	Normal	With error BI-3
$I_R(A)$	3.1383	2.9376
$I_S(A)$	3.1153	2.2624
$I_T(A)$	3.2292	2.1119
$V_{CC}(V)$	380	327
$P(KW)$	0.54	0.42

The same phenomenon is repeated at the base frequencies of 45, 47.5, 50, 52.5, 55 and 57.5 Hz when placing the short circuit in the R phase. And in fact, the short presence in the R phase affected the S and T phases. Through the analysis in Table 5, it is obvious that the extreme conditions of the test, the normal operation and the short circuit of BI-3, can easily be described in the time domain as seen at the beginning, as a low impedance short circuit of 9.26% round and this is remarkable. Even if its occurrence is controlled during tests, the potential of its intensity to destroy the device is revealed by the operation of the generator electrical system. However, in short impedance events, the unbalance of the generator is hidden and it is difficult to detect it in time domain analysis. These conditions are shown in figures 6a to p.

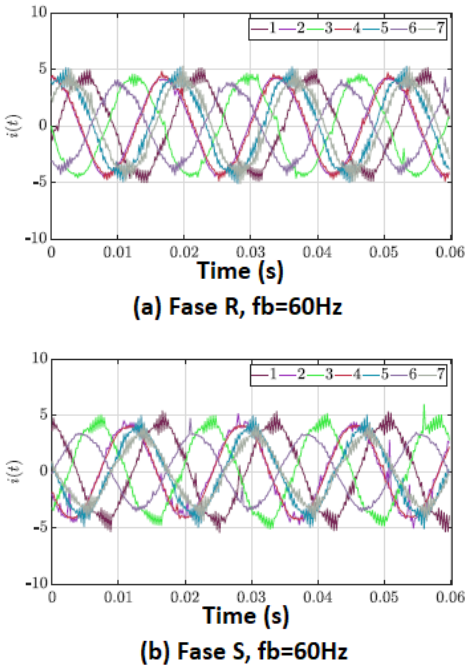

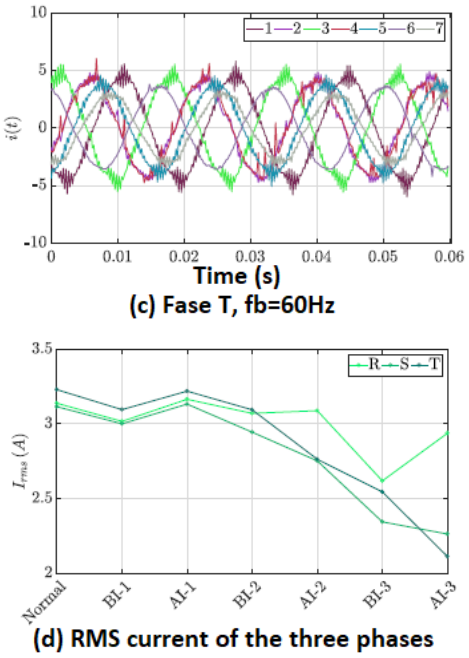

Figure 5. Comparison of the electric current of three lines, with performance close to the nominal current, in different failure conditions. Caption (1) generator in normal state, (2) failure AI-1, (3) BI-1, (4) AI-2, (5) BI-2, (6) AI-3, (7) BI-3

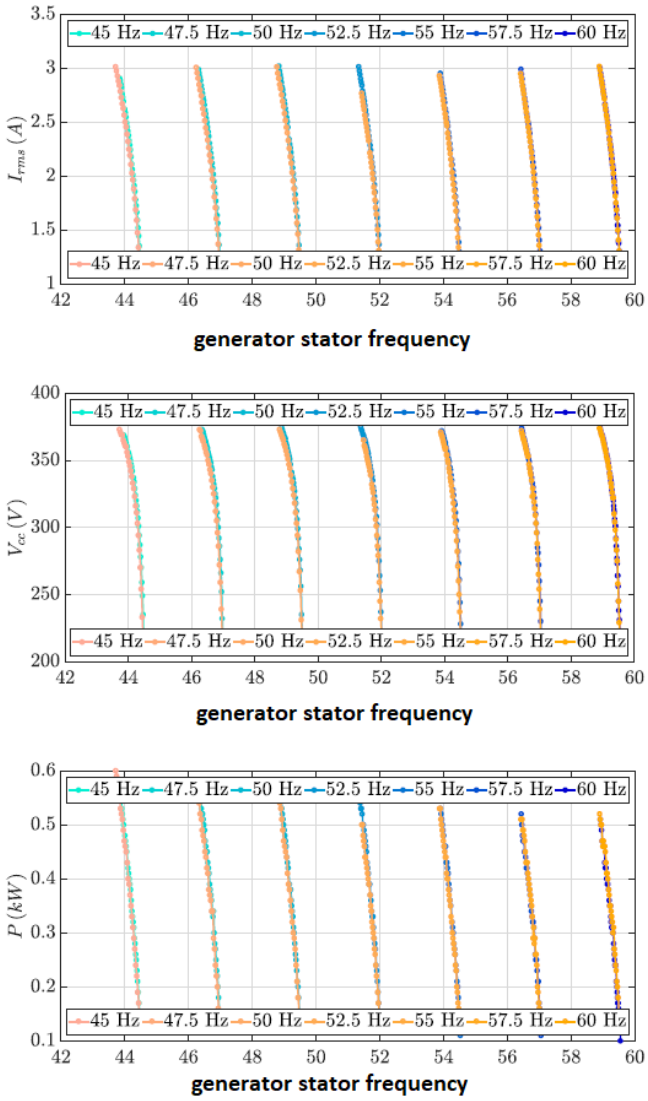

Figure 6. Corrected SCIG curves under normal conditions, in blue, and error1 CC AI-, in yellow. In 4-16A the behaviour of electric current, in 4-16B the voltage in DC Bus and in 4-16C the three-phase power is produced

Evidence of a short circuit during critical failure is noticeable in the generator curves presented in Figure 7. Bus DC voltage curves and powers are far from nominal values compared to normal conditions. However, in the event of an initial breakdown (i.e. AI-1), there is almost no difference in voltage and power, as shown in Figure 7. The power and voltage information in the DC Bus indicates the occurrence of problems in the generator, so using this information in relation to other techniques can help in identifying the failures of the induction generator.

The short circuit simulation is entered in the branch between the R and S phases and although the T phase is not short-circuited on the branch, it is believed that the appearance of a fault is perceived in all three generator currents. Feature extraction was done in phase A. Database formation is explained in the next section.

3.1. Results of applications of extractor versus classifier

Table 5 shows the general results after 50 exercises of all the extractor-classifier combinations, in the training and testing bases. Using Fourier as the feature extractor, MLP

achieved an average success rate among all classes of 84.48% and 76.53% in the training and test bases, respectively. As expected, it was better than linear classifications. Adding new features to the database provided improvements in all extractor-classifier combinations, however, it did not make the problem linearly separable, which justified the results of the OLS and Simple Perceptron classifiers reaching results below the MLP and Gaussian classifier. The sensitivity shows that MLP is better than other methods for identifying the normal operating conditions of the generator.

The feature also shows that MLP is better than other classifiers in predicting faulty conditions. Goertzel's algorithm, despite implementing Fourier transform, provided results below classical Fourier transform for MLP classifier. This is especially seen in the test base, where the difference between the results in the training and test bases is greater than that of the Fourier extractor. Obviously, with this extractor, the simple perceptron and OLS classifiers obtained much worse results than the Fourier extractor, indicating that the use of this extractor worsens the separability of the database.

Also, in Table 5, the combination of HOS-MLP ranks second in overall accuracy. There is a highlight for combining this extractor with a Gaussian classifier. This occurs because both the HOS extractor and the Gaussian classifier base their theories on Gaussian processes. The results of this extractor in linear classifiers were better than Goertzel's extractor, which indicates better resolution. SCM extractor was not effective for induction generator failure classification. Through these analyses, it was found that Fourier extractor is more effective for detecting short circuit in induction generator.

Table 5. The overall results of the extractor-classifier for the following criteria:

Accuracy (Acc), sensitivity (Sen), specificity (ESP), F score (Fsc) in training and test databases

classifier	Acc %	Sen %	ESP %	Fsc %
Training				
Fourier				
MLP	84.48 ±2.65	84.48 ±2.65	97.01 ±0.59	84.48 ±2.65
quadratic Gaussian	77.30 ±0.63	77.47 ±1.13	95.33 ±0.16	77.39 ±0.81
simple perceptron	66.56 ±1.17	67.19 ±1.71	92.43 ±0.43	67.13 ±1.37
OLS	64.91 ±0.88	65.10 ±1.03	91.73 ±0.29	65.00 ±0.87
Goertzel				
MLP	81.42 ±1.46	81.42 ±1.46	96.33 ±0.34	81.42 ±1.46
quadratic Gaussian	75.40 ±0.58	73.59 ±1.56	91.26 ±0.98	75.54 ±0.87
simple perceptron	32.80 ±2.53	33.01 ±2.71	74.66 ±2.40	33.04 ±2.73
OLS	42.48 ±0.99	42.86 ±1.19	81.64 ±0.60	42.72 ±1.03
HOS				
MLP	83.31 ±1.69	85.31 ±3.57	98.82 ±0.74	93.31 ±2.03
quadratic Gaussian	78.96 ±0.64	78.96 ±0.64	95.75 ±0.16	78.96 ±0.64
simple perceptron	49.73 ±2.61	49.75 ±2.59	85.69 ±1.54	49.91 ±2.80
OLS	59.31 ±1.26	59.67 ±1.72	89.80 ±0.51	59.58 ±1.40
SCM				
MLP	40.93 ±5.58	40.93 ±7.97	80.61 ±3.56	40.93 ±4.75
quadratic Gaussian	54.97 ±1.00	55.03 ±1.05	88.00 ±0.41	55.03 ±1.00
simple perceptron	30.75 ±1.72	31.03 ±1.71	73.21 ±1.71	31.18 ±1.64
OLS	43.62 ±0.97	43.93 ±1.36	82.34 ±0.54	43.83 ±1.08
Test				
Fourier				
MLP	76.53 ±3.45	76.98 ±3.59	95.13 ±0.87	76.79 ±3.40
quadratic Gaussian	72.32 ±2.29	72.61 ±2.42	94.09 ±0.68	72.65 ±2.36
simple perceptron	66.56 ±1.17	67.19 ±1.71	92.43 ±0.43	67.13 ±1.37
OLS	64.91 ±0.88	65.10 ±1.03	91.73 ±0.29	65.00 ±0.87
Goertzel				
MLP	65.59 ±3.16	65.59 ±3.16	92.16 ±0.94	65.92 ±2.99
quadratic Gaussian	71.30 ±0.78	70.32 ±1.21	88.57 ±0.78	71.53 ±0.54
simple perceptron	32.80 ±2.53	33.01 ±2.71	74.66 ±2.40	33.04 ±2.73
OLS	42.48 ±0.99	42.86 ±1.19	81.64 ±0.60	42.72 ±1.03
HOS				
MLP	73.54 ±1.42	73.54 ±2.31	86.82 ±0.34	73.54 ±1.57
quadratic Gaussian	76.72 ±2.13	76.94 ±2.25	95.25 ±0.59	76.97 ±2.10
simple perceptron	49.73 ±2.61	49.75 ±2.59	85.69 ±1.54	49.91 ±2.80
OLS	59.31 ±1.26	59.67 ±1.72	89.80 ±0.51	59.58 ±1.40
SCM				
MLP	57.15 ±1.52	57.24 ±1.52	88.88 ±0.62	57.20 ±1.51
quadratic Gaussian	51.49 ±2.37	52.25 ±2.87	86.73 ±1.09	52.21 ±2.42
simple perceptron	30.75 ±1.72	31.03 ±1.71	73.21 ±1.71	31.18 ±1.64
OLS	43.62 ±0.97	43.93 ±1.36	82.34 ±0.54	43.83 ±1.08

Table 6. The amount of hit according to the class of all classifiers using the Fourier extractor

Class	Training			
	MLP	quadratic Gaussian	simple perceptron	OLS
Normal	99.98± 0.11	99.14±0.33	100.00±0.00	99.81 ±0.34
AI-1	73.51± 12.26	62.94±3.27	54.05±5.85	58.51 ±4.10
AI-2	66.00± 8.74	54.11±3.28	24.68±13.85	27.86 ±5.60
AI-3	94.05± 3.82	86.71±1.31	61.57±11.78	89.68 ±1.76
BI-1	58.94± 12.36	39.49±5.91	9.51±9.82	26.30 ±0.68
BI-2	98.89± 1.12	92.10±1.21	33.29±17.12	54.08 ±3.61
BI-3	100.00 ±0.00	100.0±0.00	77.06±18.53	98.13 ±0.57
Class	**Test**			
	MLP	**quadratic Gaussian**	**simple perceptron**	**OLS**
Normal	99.25± 1.18	98.76±1.61	99.98±0.12	99.70 ±0.46
AI-1	52.16± 14.23	53.80±7.01	53.32±7.67	55.53 ±5.09
AI-2	49.96± 11.07	47.78±8.02	22.00±13.46	26.15 ±6.92
AI-3	85.58± 6.92	82.70±6.80	61.30±13.17	89.16 ±3.70
BI-1	36.94± 14.46	25.03±9.91	7.88±9.18	23.73 ±4.18
BI-2	92.44± 4.09	89.10±4.46	32.93±18.76	52.71 ±4.38
BI-3	98.81± 1.99	100.00±0.0 0	78.31±18.07	97.69 ±2.35

Table 6 shows the rate of hit based on the class of the proposed classifiers. It can be seen that in all the classifiers, the Normal class was obtained more than 98%. Class BI-3 was classified by MLP with 100% and 99.81% accuracy in training and test bases. And this was expected because this is the most critical database failure condition. Linear classifiers achieved lower success rates than MLP for other classes.

4. Conclusions

The current work deals with the prediction of wind turbine short circuit condition on the basis of neural network techniques. In fact, in all solved cases, normal conditions were classified with an accuracy above 99%, and by grouping all errors together, 100% was obtained in a dual classification. Rejection thresholds are implemented to reduce false positive and negative rates despite none of the samples being rejected. By analysing the outputs of dual neural networks, it is possible to detect when the dc bus is far from its nominal value (311 V), normal samples are usually misclassified as faulty, but the reliability of the classifier by band rejection due to classification the false positive error is maintained to avoid it. The analysis performed on the four feature extractors showed that in all the classifiers, the results of using Fourier to combine the databases are more effective, therefore, this information is relevant to perform short circuit detection in SCIG. The method used in this work proved to be efficient and can be replicated in systems already installed in wind farms as well as in a newer wind turbine. Since the frequency converters feed the new generators, this solution can also be embedded in it, creating an integrated product that is responsible for feeding, controlling and monitoring. This will certainly increase the reliability and availability of the wind farm.

References

[1] J. Shair, X. Xie, W. Liu, X. Li, and H. Li, “Modeling and stability analysis methods for investigating subsynchronous control interaction in large-scale wind power systems,” in Renew Sustain Energy Rev. vol. 135 pp. 110420, 2021.

[2] G. Rudy, and K.H. Khwee, “A new T-circuit model of wind turbine generator for power system steady state studies,” Bulletin of Electrical Engineering and Informatics. vol. 10, no.2, pp. 550-558, 2021.

[3] G.T. Enes, S. Emiroglu, and M.A. Yalcin, “Optimal DG allocation and sizing in distribution systems with Thevenin based impedance stability index,” International Journal of Electrical Power & Energy Systems, vol. 144, pp. 108555, 2023.

[4] D. Oliveira, R. Alves, and M.H. Bollen, “Susceptibility of large wind power plants to voltage disturbances-Recommendations to stakeholders,” Journal of Modern Power Systems and Clean Energy. vol. 10, no. 2. pp. 416-429, 2021.

[5] L. Trevor, “Wind energy engineering: A handbook for onshore and offshore wind turbines,” Elsevier, 2023.

[6] J.B. Francisco, “Short-circuit current contribution of doubly-fed wind turbines according to IEC and IEEE standards,” IEEE Transactions on Power Delivery. vol. 36, no. 5, pp. 2904-2912, 2020.

[7] R.M. Furlaneto, I. Kocar, A. Grilo-Pavani, U. Karaagac, A. Haddadi, and E. Farantatos, “Short circuit network equivalents of systems with inverter-based resources reference,” Electric Power Systems Research. Elsevier, vol. 199, no. 107314, 2021.

[8] F. Jimenez-Buendıa, A. Honrubia-Escribano, A. Lorenzo-Bonache, E. Artigao, and E. Gomez-Lazaro, “Short-Circuit Current Contribution of Doubly-Fed WindTurbines according to IEC and IEEE Standards,” IEEE TRANSACTIONS ONPOWER

DELIVERY. IEEE, Minneapolis, Minnesota, USA, pp. 1-10, 2020.

[9] K. Mahesh, "Optimal multi-objective placement and sizing of distributed generation in distribution system: a comprehensive review," Energies. vol. 15, no. 21, pp. 7850, 2022.

[10] A.H. Mohammadzadeh Niaki, and A.H. Solat, "A Novel Method to Determine the Maximum Penetration Level of Distributed Generation in the Distribution Network," 2020 28th Iranian Conference on Electrical Engineering (ICEE). IEEE, 2020.

[11] S.H. Abdurrahman, Y. Sun, and Z. Wang, "Optimization techniques applied for optimal planning and integration of renewable energy sources based on distributed generation: Recent trends," Cogent Engineering. vol. 7, no. 1, pp. 1766394, 2020.

[12] D. Mohammad, Z. Montazeri, and O.P. Malik, "Optimal sizing and placement of capacitor banks and distributed generation in distribution systems using spring search algorithm," International Journal of Emerging Electric Power Systems. vol. 21, no. 1, pp. 20190217, 2020.

[13] K. Eshan, "The optimal placement and sizing of distributed generation in an active distribution network with several soft open points," Energies, vol. 14, no. 4, pp. 1084, 2021.

[14] E.M. Hemmat, "Investigation of best artificial neural network topology to model the dynamic viscosity of MWCNT-ZnO/SAE 5W30 nano-lubricant," Materials Today Communications. vol. 35, pp. 106074, 2023.

[15] E.M. Hemmat, "A well-trained artificial neural network for predicting the optimum conditions of MWCNT–ZnO (10: 90)/SAE 40 nano-lubricant at different shear rates, temperatures, and concentration of nanoparticles," Arabian Journal of Chemistry. vol. 16, no. 2, pp. 104508, 2023.

[16] G.M. Mahdi, "Considering transient short-circuit currents of wind farms in overcurrent relays coordination using binary linear programming," International Journal of Electrical Power & Energy Systems. vol. 131, pp. 107086, 2021.

[17] C. Pedro, "A comprehensive overview of power converter applied in high-power wind turbine: Key challenges and potential solutions," IEEE Transactions on Power Electronics. vol. 38, no. 5, pp. 6169-6195, 2023.

[18] E.M. Hemmat, "Designing the best ANN topology for predicting the dynamic viscosity and rheological behavior of MWCNT-CuO (30: 70)/SAE 50 nano-lubricant," Colloids and Surfaces A: Physicochemical and Engineering Aspects. vol. 651, pp. 129691, 2022.